Review

Hunting Quantum Gravity with Analogs: The Case of High-Energy Particle Physics

Paolo Castorina [1,2,*], **Alfredo Iorio** [2] and **Helmut Satz** [3]

1   Istituto Nazionale di Fisica Nucleare, Sezione di Catania, I-95123 Catania, Italy
2   Faculty of Mathematics and Physics, Charles University, V Holešovičkách 2, 18000 Prague 8, Czech Republic
3   Fakultät für Physik, Universität Bielefeld, D-33501 Bielefeld, Germany
*   Correspondence: paolo.castorina@ct.infn.it

Abstract: In this review, we collect, for the first time, old and new research results, and present future perspectives on how hadron production, in high-energy scattering processes, can experimentally probe fundamental questions of quantum gravity. The key observations that ignited the link between the two arenas are the so-called "color-event horizon" of quantum chromodynamics, and the (de)accelerations involved in such scattering processes. Both phenomena point to the Unruh (and related Hawking)-type effects. After the first pioneering investigations, such research studies continued, including studies of the horizon entropy and other "black-hole thermodynamical" behaviors, which incidentally are also part of the frontier of the analog gravity research itself. It has been stressed that the *trait d'union* between the two phenomenologies is that in both hadron physics and black hole physics, "thermal" behaviors are more easily understood, not as due to real thermalization processes (sometimes just impossible, given the small number of particles involved), but rather to a stochastic/quantum entanglement nature of such temperatures. Finally, other aspects, such as the self-critical organizations of hadronic matter and of black holes, have been recently investigated. The results of those investigations are also summarized and commented upon here. As a general remark, this research line shows that we can probe quantum gravity theoretical constructions with analog systems that are not confined to only the condensed matter arena.

Keywords: analogs; hadronic physics; quantum gravity

1. Introduction

Analogs have reached a level of maturity in theoretical modeling, e.g., [1], and experimental modeling, e.g., [2], which might bring them to the forefront in the experimental search for quantum gravity (QG) signatures, or, in general, in the theoretical research in fundamental high-energy physics, see, e.g., the contribution [3] to this Issue.

There are two obstacles. First, there is the skepticism of a large part of the theoretical community, which still do not trust analogs as a way to test the fundamental ideas; second, the need for a new era in the analog enterprise, namely to reach *dynamical* effects, rather than *kinematical* effects [1].

Here, we describe a line of research, initiated in [5,6], which addresses both problems. We focus on a specific high-energy scenario, where the effects of a large acceleration are evident; much of the subsequent work was carried out to understand the meaning of entropy in this context and its relation to BH entropy, which is a typical dynamical issue (e.g., recall that Wald's formula relates entropy to the action [7]).

The reproduction of aspects of gravitational physics, both classical and quantum, by means of analogs, is mainly based on condensed matter systems. Examples range from lasers [8–12] (see also the contribution [13] to this issue) to water-waves [14], and from Bose–Einstein condensates [2] to graphene [15–25], and more [1].

In particular, the detection of some form of the Unruh phenomenon [26–28] has been proposed in various set-ups [8–11,14,17,18,29–31]. However, in many of the proposed analog systems, the Unruh temperature

$$T_U = \frac{\hbar a}{2\pi c k_B} \tag{1}$$

is still too small [5] for a direct experimental verification, as one sees that $1 \text{ m/s}^2 \rightarrow \sim 4 \times 10^{-21}$ K. In (1), a is the uniform acceleration, and we explicitly kept the Planck constant, the speed of light, and the Boltzmann constant to ease the unit conversion. In the following, we shall set to one $\hbar, c$ and k_B.

Some encouraging results come from femtosecond laser pulses that can produce an acceleration $a \simeq 10^{23}$ m/s^2 [11], with the associated Unruh temperature $T_U \sim 400$ K. On the other hand, the enormous accelerations (or decelerations) produced in relativistic heavy ion collisions, $a \simeq 4.6 \times 10^{32}$ m/s^2, have associated Unruh temperatures many orders of magnitude larger, $T_U \sim 1.85 \times 10^{12}$ K. A simple unit conversion shows that this is nothing else than the hadronization temperature T_h

$$T_U \sim 160 \text{ MeV} \sim T_h \,. \tag{2}$$

This fact triggered the investigation of hadron production, in high-energy collisions, as a manifestation of the Unruh phenomenon in quantum chromodynamics (QCD) [5,6].

Of the latter we discuss it in this paper, by reviewing why such an interpretation is natural, commenting on the various ramifications, and speculating on the possible future directions. In other words, we elaborate on which aspects of this QCD phenomenology can be taken as viable analogs of specific aspects of QG.

The underlying idea behind the latter analogies is based on quark confinement as a phenomenon where a "horizon" (sometimes called "color horizon", see, e.g., [32,33]) hides those degrees of freedom to any observer, and only quantum (tunneling) effects could explain a radiation phenomenon [5]. This is a non-perturbative quantum phenomenon, related to the chromomagnetic properties of the QCD vacuum (see for example reference [34]), producing the squeezing of the chromoelectric field in quark–antiquark strings, with a constant energy density. Let us comment a bit more on this.

Quark confinement can be described as due to a potential that grows linearly at large distances, $V = \sigma r$. This corresponds to a constant acceleration; henceforth, the Rindler spacetime is the appropriate framework for this phenomenon. As well known, the Rindler metric is equivalent to the near-horizon approximation of the BH metric, with the acceleration equal to the surface gravity, k. Therefore, the *local* correspondence between a linear potential and the near-horizon dynamics of a BH is a strong analogy.

This is another perspective as to why quark confinement can be related to a "color horizon" [32,33], which hides the color degrees of freedom and a Rindler horizon, and is, in turn, associated with a specific BH (in [35], some proposals of specific BHs could account for this specific scenario). On the other hand, the Hawking radiation is a quantum phenomenon associated with tunneling and pair creation near the event horizon [36,37]. This is a clear dynamical correspondence to the string-breaking and quark–antiquark pair creation in the final process of the mechanism leading from the color degrees of freedom until the formation of hadrons.

Finally, another delicate dynamical issue involves the entropy associated with a "color event horizon". This is an entanglement entropy between the quantum field modes on the two sides of the horizon. As well known, such an entropy follows an area law [38–40], similar to the entropy of a BH [41,42], when logarithmic corrections are not included, or the entropy of a Rindler horizon [43]. Even though it is still an open question whether entanglement entropy alone could account for the whole BH entropy, this is yet another argument that strengthens the analogy between the two systems. Furthermore, in such QCD environments, the entropy is a quantity routinely considered, e.g., in (quantum) statistical

models. Henceforth, we have measurable and natural candidates for quantities that can play the role of a BH entropy. As mentioned earlier, this is a very important milestone to move analogs to the next era; that is, the possibility to reproduce BH thermodynamics, with its intriguing fundamental open questions, such as the information paradox. For the sake of completeness, let us recall that the general Page approach (i.e., to the calculation of the entanglement entropy of an evaporating BH [44]) has been successfully applied to gluon shadowing in deep inelastic scattering [45], following the proposal in [46].

In this review paper, we collect, for the first time, the most important (old and new) results of this line of research; we comment on and discuss them. The paper is organized as follows. In Section 2, we recall the main features of the Unruh effect, and of the related BH physics, using the descriptions of the effects that make the link with hadron physics (that we want to disclose) easier; this Section is also important for setting the notation. In Section 3, we recollect three well-known aspects of the phenomenology of hadrons, which will be scrutinized using the analogies and links with gravitational physics in the Sections that follow. The hadronic phenomena described in Section 3.1 are reinterpreted as gravity analogs in Section 3.2; the hadronic phenomena described in Section 4 are reinterpreted as gravity analogs in Section 4.2; finally, the hadronic phenomena described in Section 5 are reinterpreted as gravity analogs in Section 5.2. We close the review with our conclusions in Section 6.

2. Accelerated Observers and near BH Horizon Observers

In this Section, we recall the main features of the Unruh effect, and the related BH physics, which will mostly be used in the realizations in hadronic physics, which we discuss later. In particular, we first discuss the interplay between pair production, tunneling, and the Unruh effect. We then mention the correspondence between the near-horizon BH metric and Rindler metric, and the area law obeyed by BH entropy.

Let us begin by discussing the Unruh effect and its relation to tunneling and pair production. For this part, we follow [5].

Consider the action, A, of a particle of mass m, subject to a constant force derived from a potential $\varphi(x)$:

$$A = -\int (m \, ds + \varphi \, dt).$$ (3)

For a constant force, the one-dimensional (1D) potential is $\varphi = -\sigma x$ modulo, an additive constant, and the equations of motion of the particle are

$$\frac{dp_x}{dt} = \sigma, \quad \frac{dp_\perp}{dt} = 0.$$ (4)

Using $ds^2 = (1 - v^2(t)) \, dt^2$ and the equations of motion, one can evaluate action A [5]

$$
\begin{aligned}
A(\tau) &= \int^\tau dt \left(-m \sqrt{1 - v(t)^2} + \sigma x(t) \right) \\
&= -\frac{m}{a} \operatorname{arcsinh}(a\tau) + \frac{\sigma}{2 a^2} \left[a \tau \left(\sqrt{1 + a^2 \tau^2} - 2 \right) + \operatorname{arcsinh}(a \tau) \right] + \text{const}.
\end{aligned}
$$ (5)

In quantum theory, the particle has a finite probability to be found under the potential barrier, σx, in the classically forbidden region. Mathematically, this comes about because action A, being an analytic function of τ, has an imaginary part

$$A(\tau) = \frac{m \pi}{a} - \frac{\sigma \pi}{2 a^2} = \frac{\pi m^2}{2\sigma}, .$$ (6)

which corresponds to the motion of a particle in Euclidean time, t_E, with the Euclidean trajectory

$$x(t_E) = a^{-1} \left(\sqrt{1 - a^2 t_E^2} - 1 \right),$$ (7)

bouncing between the two identical points $x_a = -a^{-1}$ at $t_{E,a} = -a^{-1}$ and $x_b = -a^{-1}$ at $t_{E,b} = a^{-1}$, and the turning point $x_a = 0$ at $t_{E,a} = 0$.

In the quasi-classical approximation, the rate of tunneling under the potential barrier is given by

$$\Gamma_{vac \to m} \sim e^{-2\operatorname{Im}A} = e^{-\frac{\pi m^2}{\sigma}}, \tag{8}$$

which gives the probability to produce a particle and its antiparticle (each of mass m) out of the vacuum, under the effects of a constant force σ. The ratio of the probabilities to produce states of masses M and m is then

$$\frac{\Gamma_{vac \to M}}{\Gamma_{vac \to m}} = e^{-\frac{\pi(M^2 - m^2)}{\sigma}}. \tag{9}$$

The relation (9) had a double interpretation, in terms of both the Unruh and the Schwinger effects, see, e.g., [47–49] and references therein. Indeed, consider a detector with quantum levels m and M, moving with a constant acceleration. Each level is accelerated differently; however, if the splitting is not large, $M - m \ll m$, we can introduce the average acceleration of the detector

$$\bar{a} = \frac{2\sigma}{M + m}. \tag{10}$$

Substituting (10) into (9), we arrive at

$$\frac{\Gamma_{vac \to M}}{\Gamma_{vac \to m}} = e^{\frac{2\pi(M-m)}{\bar{a}}}. \tag{11}$$

This expression is reminiscent of the Boltzmann probabilistic weight in a heat bath, with an effective temperature, $T = \bar{a}/2\pi$. This is the Unruh effect.

A similar study of the Unruh radiation (tunneling through a barrier by WKB-like methods) was carried out in [50]. A more rigorous derivation of the Unruh effect can be given by recalling that the uniformly accelerated detector in the Minkowski space is equivalent to the inertial detector in the Rindler space. The vacuum in the Minkowski space is related to the vacuum in the Rindler space by a nontrivial Bogoliubov transformation, which shows that the Rindler vacuum is populated with thermal radiation of temperature $T = a/2\pi$ (for a review, see [28]).

We will now focus on another aspect of the Hawking–Unruh phenomenon that is crucial for the analogy between quark confinement and the physics of curved spacetime (which we shall discuss later)—the correspondence between the Rindler metric and the near-horizon approximation of a BH metric.

The Schwarzschild metric for a BH of mass M, in radial coordinates, is given by

$$ds^2 = f(r)dt^2 - f(r)^{-1}dr^2 - r^2[d\theta^2 + \sin^2\theta d\phi^2], \tag{12}$$

with

$$f(r) = \left(1 - \frac{2GM}{r}\right). \tag{13}$$

The equation $f(r) = 0$ sets the Schwarzschild radius, R_S, as the radius of the spherical event horizon

$$R_S = 2GM. \tag{14}$$

This means that $M(R_S) = (2G)^{-1} R_S$, which is a linear law for the BH mass. This is particularly interesting if one notices that an analogous behavior is enjoyed by the confining potential of the strong interactions.

In Equation (12), the coordinate transformation [39] is

$$\eta = \frac{\sqrt{f(r)}}{\kappa}, \tag{15}$$

where the surface gravity κ is given by

$$\kappa = \frac{1}{2} \left(\frac{\partial f}{\partial r} \right)_{r=R_S}, \tag{16}$$

one obtains, for $r \to R_S$, the BH metric in the near-horizon approximation

$$ds^2 = \eta^2 \kappa^2 dt^2 - d\eta^2 - R^2(d\theta^2 + sin^2\theta d\phi^2). \tag{17}$$

To compare the previous result with the Rindler metric of a constantly accelerated observer, let us recall the relations among Rindler coordinates, (ξ, τ) and the Minkowski coordinates (x, t)

$$x = \xi \cosh a\tau, \quad t = \xi \sinh a\tau, \tag{18}$$

where $a = \sigma/m$ denotes the acceleration in the instantaneous rest frame of m, and τ is the proper time. With these, the metrics of such an accelerating system (in spherical coordinates) are

$$ds^2 = \xi^2 a^2 d\tau^2 - d\xi^2 - \xi^2 \cosh^2 a\tau (d\theta^2 + \sin^2\theta d\phi^2). \tag{19}$$

Comparing Equations (19) and (17), it is evident that the system in uniform acceleration is the same as a system near a spherical BH horizon, provided we identify the surface gravity κ with the acceleration a.

The final topic of this Section will be entropy and its area law, a feature common to BH and constantly accelerated systems.

The gravitational entropy is related to the existence of a horizon, which forbids an observer to acquire knowledge (or what is happening beyond it). In a way, it could be seen as a measure of the ignorance of the fate of matter (and space) degrees of freedom that contribute to making the BH.

As well known, such entropy obeys the Bekenstein–Hawking area law [41,42]:

$$S_{\text{BH}} = \frac{1}{4} \frac{A}{\ell_P^2}, \tag{20}$$

where $\ell_P = \sqrt{G}$ is the Planck length, and, for Schwarzschild BH: $A = 4\pi R_S^2$. Once more the only parameter of interest is the mass of the BH: $M \sim R_S$.

On the other hand, it is also well known that access to the degrees of freedom describing an accelerated observer is also restricted by a horizon—the Rindler horizon. Therefore, the entropy of the so-called Rindler wedge was evaluated (similar to the BH). The computation was performed a long time ago [43], and it turns out that $S = (1/4) (A_a/\ell_P^2)$, where A_a is the area of a surface of the constant Rindler spatial coordinate, x, and the proper time, τ. If *yandz* are the Minkowski coordinates (we suppose that the acceleration is along the x-axis), the entropy is actually infinite; however, an entropy *density*, per unit area, can be defined for this spacetime.

Finally, we recall another well-known result, namely that the entanglement (hence, quantum) entropy of a bipartite system (which includes both the Rindler and the BH cases just discussed, due to their event horizons) also obeys an area law. This has been shown in various quantum field theoretical setups, see, e.g., [38–40].

In the following, we schematically recall those results of the phenomenological analysis of high-energy collision data, which will then be reconsidered in light of the gravity analog, in a separate dedicated Subsection.

3. Hadron Production in High-Energy Collisions

3.1. Statistical Hadronization Model

There is abundant multihadron production in high-energy collisions, starting from the electron-positron annihilation, and then in the proton–proton, proton–nucleus, and nucleus–nucleus scattering processes. The relative rates of the secondaries produced are well accounted for by ideal gases of all hadrons and hadronic resonances, at a fixed temperature T and baryochemical potential μ_B. This is known as the statistical hadronization model (SHM) [51–53]. There is one (well-known) caveat though. The strangeness production one finds is reduced with respect to the rates predicted by the SHM. However, this suppression can be taken into account by one further parameter, $0 < \gamma_s \leq 1$, if the predicted rate for a hadron species containing $\nu = 1, 2, 3$ strange quarks is suppressed by the factor γ_s^ν [54].

To describe such a resonance gas, the basic tool one needs is the grand-canonical partition function for an ideal gas at the temperature T in a spatial volume V

$$\ln Z(T) = V \sum_i \frac{d_i \gamma_s^{\nu_i}}{(2\pi)^3} \, \phi(m_i, T) \,, \tag{21}$$

with d_i specifying the degeneracy (spin, isospin) of the species i, and m_i its mass. The sum runs over all species. For simplicity, we assume for the moment $\mu_B = 0$. Here,

$$\phi(m_i, T) = \int d^3 p \, \exp\{\sqrt{p^2 + m_i^2}/T\} \sim \exp(-m_i/T) \,, \tag{22}$$

is the Boltzmann factor for species i, so that the ratio of the production rates, N_i and N_j, for hadrons of species i and j, is given by

$$\frac{N_i}{N_j} = \frac{d_i \gamma_s^{\nu_i} \phi(m_i, T)}{d_j \gamma_s^{\nu_j} \phi(m_j, T)} \,, \tag{23}$$

where $\nu_i = 0, 1, 2, 3$ specifies the number of strange quarks in species i.

Both the temperature T and strangeness suppression factor γ_s were measured, at various collision energies, and for different collision configurations. The resulting temperature of the emerging resonance gas is found to have a universal value

$$T_c \simeq 160 \pm 10 \, \text{MeV} \,, \tag{24}$$

for all (high) collision energies, where $\mu_B \simeq 0$ and all collision configurations, including hadron production in the $e^+ e^-$ annihilation.

Moreover, in heavy ion collisions at lower energy, the finite baryon density has a crucial role and the dynamics are dominated by Fermi statistics and baryon repulsion. In the $T - \mu_B$ plane, the dependence of the hadronization temperature on μ_B defines the chemical "freeze-out" curve, which can be described by specific (but poorly understood, see next Section) criteria [55–59].

Indeed, a fixed ratio between the entropy density, s, and the hadronization temperature, $s/T^3 \simeq 7$, or the average energy per particle, $< E > /N \simeq 1.08$ GeV reproduces the curve in the $T - \mu_B$ plane, as shown in Figure 1, where the percolation model result [55] is also plotted.
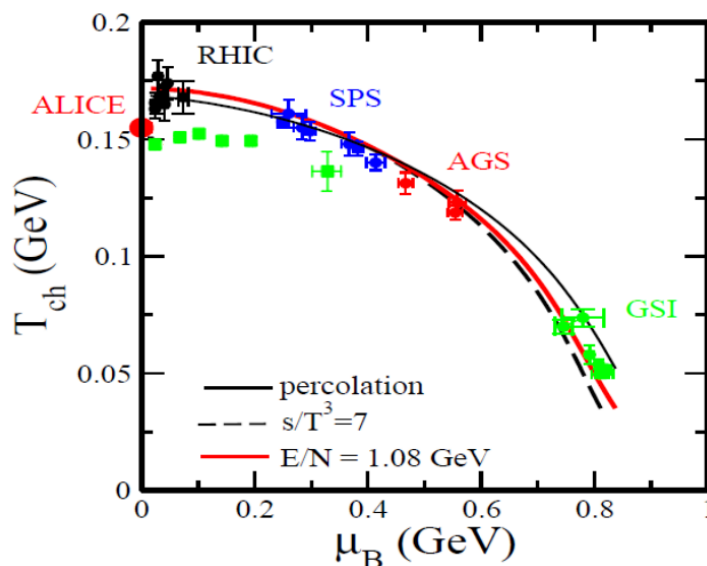
Figure 1. Freeze-out curve in the statistical hadronization model compared with the criteria discussed in the text. The green squares without error bars are the QCD lattice simulation data.

The agreement of the SHM with data on the abundances of different hadronic species, from e^+e^- annihilation to heavy ion collisions, is puzzling. In heavy ion collisions, it is possible to expect the emergence of statistical distributions as a result of intense reinteractions; however, this seems very implausible in the e^+e^- annihilation at high energies because the density of the produced hadron is small there.

Moreover, in e^+e^-, the jet structure, the angular distributions of the produced hadrons, and the inter–jet correlations, point to the important role of QCD dynamics of gluon radiation. Thus, the "phase space dominance" cannot be invoked. Indeed, in all high-energy collisions, for $\sqrt{(s)} \geq 20$ GeV, the hadronization temperature is essentially constant and independent from the initial configurations.

The previous aspects call for some *universal* mechanism at the root of hadron production, which has to be related to the way the QCD vacuum responds to color fields.

3.2. Analog Gravity Interpretation of the SHM and the QCD Hawking–Unruh Radiation

As mentioned in the introduction, the phenomenology of quark confinement can be seen as the effect of a Rindler force due to the string tension, σ. Let us now describe this phenomenon in more detail.

We recall in Section 2 that the basic mechanism of the Unruh radiation involves tunneling through the confining event horizon. This is most simply illustrated by hadron production through the e^+e^- annihilation into a q pair, see Figure 2.
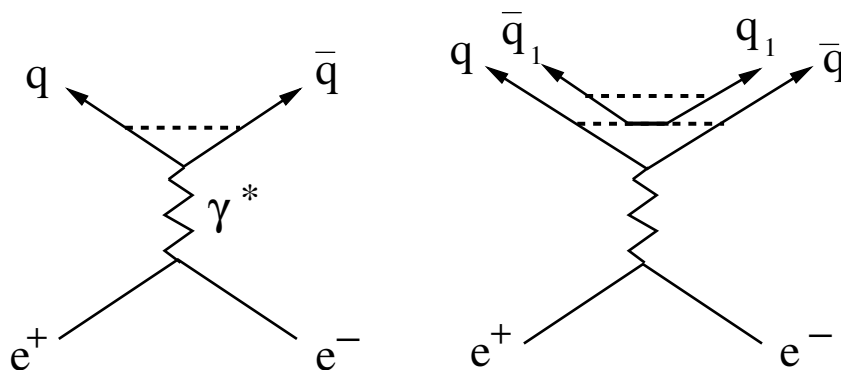

Figure 2. Quark formation in the e^+e^- annihilation

The first quark–antiquark pair, $q\bar{q}$, initially tries to separate. The attempt stops when both quarks hit the confinement horizon, i.e., when they both reach the end of the binding string, where their separation is R. At that point, the attempt to separate can only continue if a further quark–antiquark system is excited from the vacuum. Although the new pair, $q_1\bar{q}_1$, is at rest, in the overall center of mass system, each constituent has a transverse momentum k_T, determined by the uncertainty relation in terms of the transverse dimension of the string flux tube. The string theory [60] for the basic thickness gives

$$r_T = \sqrt{2/\pi\sigma}\,, \tag{25}$$

leading to

$$k_T = \sqrt{\pi\sigma/2}\,. \tag{26}$$

The maximum separation distance R is specified by

$$\sigma R = 2\sqrt{m_q^2 + k_T^2} = 2k_T\,, \tag{27}$$

where we take $m_q = 0$ for the quark mass. From this, we obtain

$$R = \sqrt{2\pi/\sigma}\,, \tag{28}$$

as the string-breaking distance. The departing quark q now pulls the newly formed $\bar{q}_1$ along, giving it an acceleration [6]

$$a = \sqrt{2\pi\sigma}\,. \tag{29}$$

The $q_1\bar{q}_1$ pair eventually suffers the same fate as the q pair: it is separated to its confinement horizon, where it again excites a new pair, which is now emitted as the Unruh radiation of temperature

$$T_h = a/2\pi = \sqrt{\sigma/2\pi}\,, \tag{30}$$

that is also the hadronization temperature, as we shall see in a moment. This process is sequentially repeated until the energies of the initial "driving" quarks q and $\bar{q}$ are exhausted.

The case of the e^+e^- annihilation corresponds to baryochemical potential, $\mu_B = 0$. Here, one finds the average value $\sigma \simeq 0.19 \pm 0.03$ GeV^2, see, e.g., [61], which with Equation (30) then leads to

$$T_h(\mu_B = 0) = \sqrt{\sigma/2\pi} \simeq 175 \pm 15\ \text{MeV}\,. \tag{31}$$

for the freeze-out temperature at $\mu_B = 0$.

The fundamental mechanism in the Unruh scenario is quark (de)acceleration, leading to the string-breaking with the resulting pair production, as specified by Equation (27). As long as we assume a vanishing quark mass, the only dimensional parameter in the entire formalism is the string tension σ.

Therefore, the Unruh hadronization temperature is "universal"; this explains the observation of thermal hadron production in high-energy collisions in e^+e^- and pp interactions. In this respect, the emitted hadrons are "born in equilibrium" [62,63].

The previous analysis shows that the hadronization temperature corresponds to the Unruh temperature related to the string-breaking in high-energy collisions, where $\mu_B \simeq 0$.

As discussed, the dependence of the hadronization temperature on μ_B defines the chemical "freeze-out" curve, which turns out to be in agreement (see Figure 1) with a fixed ratio between the entropy density, s, the hadronization temperature, $s/T^3 \simeq 7$, and/or the average energy per particle, $< E > /N \simeq 1.08$ GeV, and/or $n \simeq 0.12$ fm^{-3}, where n is the number density.

Although the Unruh mechanism and the string-breaking provide theoretical bases for the production of newly formed hadrons in high-energy collisions, they do not address the roles of the nucleons already present in the initial state of the heavy ion collisions. However,

the corresponding hadron formation gives clear meaning to the figures that characterize the whole freeze-out curve.

Indeed, as discussed in [64], the energy of the pair produced by string-breaking, i.e., of the newly formed hadron, is given by (cf Equations (26) and (27))

$$E_h = \sigma R = \sqrt{2\pi\sigma} \,. \tag{32}$$

In the central rapidity region of high-energy collisions, one has $\mu_B \simeq 0$, so that E_h is, in fact, the average energy $\langle E \rangle$ per hadron, with an average number $\langle N \rangle$ of newly produced hadrons. Hence, one obtains

$$\frac{\langle E \rangle}{\langle N \rangle} = \sqrt{2\pi\sigma} \simeq 1.09 \pm 0.08 \, \text{GeV} \,, \tag{33}$$

in accordance with the phenomenological fit obtained from the species abundances in high-energy collisions [56,58].

Next, we turn to the number density. For a single string-breaking, the number density is given by

$$n_{sb} \simeq \frac{1}{4\pi R^3/3} \,, \tag{34}$$

where R is the string-breaking distance, which turns out to be $R = 1/T_h$ for massless quarks. For $T_h \simeq 160$ MeV, consistent with our previous evaluation, one obtains $n_{sb} \simeq 0.129$ fm^{-3}.

Let us now consider the entropy. Since the event horizon is caused by color confinement, such entropy is an entanglement entropy of quantum field modes on both sides of the horizon (recall that, here, we have no real gravitational degrees of freedom). Its general form is [39,40]

$$S_{\text{ent}} = \alpha \frac{A}{r^2} \,, \tag{35}$$

where A is the area of the event horizon, r the scale of the characteristic quantum fluctuations, and α an undetermined numerical constant, which might as well be infinite. This expression shares the holographic structure (holography of entanglement entropy is a general result, see [38,65]) with the Bekenstein–Hawking entropy [41,42] for a BH given in (20)

$$S_{\text{BH}} = \frac{1}{4} \frac{A}{\ell_P^2} \,.$$

A relation similar to (20) also holds in the case of an accelerated observer [43]. Here, we take it to be valid in our case, where gravity is not involved and the entire entropy must be of the entanglement type. The scale of the characteristic quantum fluctuations is now given by the transverse string thickness in Equation (25), rather than the Planck length, ℓ_P, of the gravitational phenomena. One obtains

$$S_h = \frac{1}{4} \frac{A_h}{r_T^2} = \frac{1}{4} \frac{4\pi R^2}{r_T^2} \,, \tag{36}$$

for the entropy in the hadron production. The parameter R is given by Equation (28), and inserting these expressions into Equation (36) for the entropy associated with the hadron production gives

$$S_h = \pi^3 \,, \tag{37}$$

and the entropy *density*, $s = S_h/V$ (here, $V = 4/3\pi R^3$), divided by T^3, turns out to be

$$\frac{s}{T^3} = \frac{S_h}{(4\pi/3)R^3 T^3} = \frac{3\pi^2}{4} \simeq 7.4 \,, \tag{38}$$

as the freeze-out condition in terms of $s(T)$ and T. This result is in accordance with the value obtained for s/T^3 from species abundance analyses in terms of the ideal resonance gas model [58,59]. Moreover, within this picture, one can show [66] that QCD entropy, evaluated by lattice simulations in the region $T_c < T < 1.3T_c$, is in reasonable agreement with a melting color event horizon.

The analogy between the freeze-out temperature as a function of μ_B and the Hawking temperature for charged BH is discussed in [6]; another interesting aspect is that it can be translated to the temperature dependence on the collision energy $\sqrt{s}$, by considering $\mu_B(\sqrt{s})$ [67].

Since the Unruh temperature triggers the search for the gravitational BH, which in its near-horizon approximation better simulates the hadronization phenomenon, one can study which BH behind that Rindler horizon could reproduce the experimental behavior of $T(\sqrt{s})$. Although the complete hadronization process is in 4D spacetime, the hadronic Rindler spacetime should be better consider as the near-horizon approximation of the effective two-dimensional (2D) BH analog for the following two reasons

- New particle creation is effectively 2D because it can be described in terms of the evolution in time of the hadronic strings, which are one-dimensional objects [68].
- The near-horizon field dynamics are effectively 2D [36,69].

Provided certain natural assumptions hold, it has been shown [35] that the so-called exact string BH in 2D dilaton gravity [68] turns out to be the best candidate, as it fits the available data on $T(\sqrt{s})$, and that its limiting case, the Witten BH, is the unique candidate to explain the constant T for all elementary scattering processes at large energies.

To conclude this Section, we now turn to the strange quark mass and the interpretation *alla* Unruh of the strangeness enhancement.

At the beginning of this Section, we illustrated how the thermal hadron production process is a Hawking–Unruh mechanism. In doing so, we neglected the effects of the quark mass. If one includes them, the expression one obtains for acceleration is

$$a_q = \frac{\sigma}{w_q} = \frac{\sigma}{\sqrt{m_q^2 + k_q^2}}, \tag{39}$$

where $w_q = \sqrt{m_q^2 + k_q^2}$ is the effective mass of the produced quark, with m_q the bare quark mass, and k_q the quark momentum inside the hadronic system $q_1\bar{q}_1$ or $q_2\bar{q}_2$ (see Figure 3). Since the string breaks [6] when it reaches a separation distance

$$x_q \simeq \frac{2}{\sigma}\sqrt{m_q^2 + \frac{\pi\sigma}{2}}, \tag{40}$$

the uncertainty relation gives us $k_q \simeq 1/x_q$

$$w_q = \sqrt{m_q^2 + [\sigma^2/(4m_q^2 + 2\pi\sigma)]}, \tag{41}$$

for the effective mass of the quark. The resulting Unruh temperature depends on the quark mass; thus it is given by

$$T(qq) \simeq \frac{\sigma}{2\pi w_q}. \tag{42}$$

Here, it is assumed that the quark masses for q_1 and q_2 are equal. For $m_q \simeq 0$, Equation (42) reduces to $T(00) \simeq \sqrt{\sigma/2\pi}$, as obtained in Equation (30).
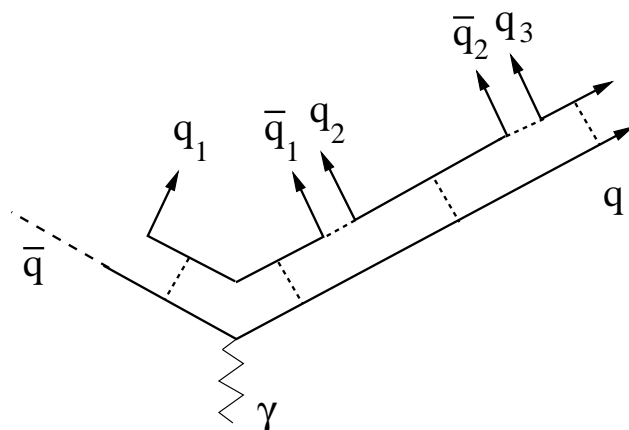
Figure 3. Sequential quark formation in the e^+e^- annihilation

If the produced hadron $\bar{q}_1 q_2$ consists of quarks of different masses, the resulting temperature has to be calculated as an average of the different accelerations involved. For one massless quark ($m_q \simeq 0$) and one of strange quark of mass m_s, the average acceleration becomes

$$\bar{a}_{0s} = \frac{w_0 a_0 + w_s a_s}{w_0 + w_s} = \frac{2\sigma}{w_0 + w_s} . \tag{43}$$

From this, the Unruh temperature of a strange meson is given by $T(0s) \simeq \sigma/\pi(w_0 + w_s)$ with $w_0 \simeq \sqrt{1/2\pi\sigma}$ and w_s is given by Equation (4) with $m_q = m_s$. Similarly, we obtain $T(ss) \simeq \sigma/2\pi w_s$ for the temperature of a meson consisting of a strange quark–antiquark pair (ϕ).

The scheme is readily generalized to baryons. The production pattern leads to an average of the accelerations of the quarks involved [70]. Thus, we have $T(000) = T(0) \simeq \sigma/2\pi w_0$ for nucleons, $T(00s) \simeq 3\sigma/2\pi(2w_0 + w_s)$ for Λ and Σ production, $T(0ss) \simeq 3\sigma/2\pi(w_0 + 2w_s)$ for Ξ production, and $T(sss) = T(ss) \simeq \sigma/2\pi w_s$ for that of Ωs.

Thus, we obtain a resonance gas picture with five different hadronization temperatures, as specified by the strangeness content of the hadron in question: $T(00) = T(000)$, $T(0s)$, $T(ss) = T(sss)$, $T(00s)$, and $T(0ss)$.

In other words, the event horizon of the color confinement leads to thermal behavior, but the resulting temperature depends on the strange quark content of the produced hadrons, causing a deviation from the full equilibrium and, hence, a suppression of strange particle production, without the introduction of the γ_s parameter. The resulting formalism was applied to the multihadron production in the e^+e^- annihilation over a wide range of energies to make a comprehensive analysis of the data, in the conventional (i.e., with γ_s) SHM and its modified Hawking–Unruh formulation [70,71]. The modified SHM, with the different Unruh temperature, gives a better fit with respect to the standard SHM formulation.

In the Hawking–Unruh formulation, the number of free parameters of the model does not increase since all previous temperatures were completely determined by the string tension and the strange quark mass. Apart from possible variations of the quantities of σ and m_s, the description is parameter-free.

In all cases, the temperature for a hadron carrying nonzero strangeness was lower than that of non-strange hadrons and this led to an overall strangeness suppression in elementary collisions, in good agreement with the data, without the introduction of the ad hoc parameter γ_s. Figure 4 reports the comparison between the SHM with one temperature and γ_s and the Hawking–Unruh-inspired approach.
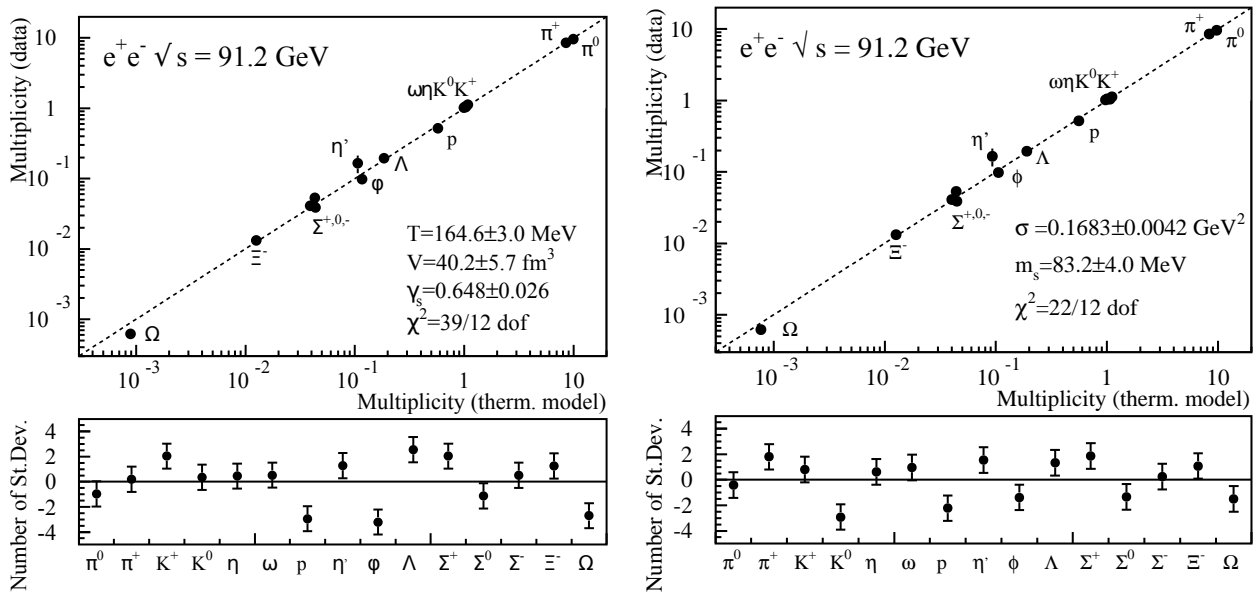
Figure 4. Comparison between the measured and fitted multiplicities of long-lived hadronic species in e^+e^- collisions at $\sqrt{s} = 91.25$ GeV. (**Left**): statistical hadronization model with one temperature. (**Right**): Hawking–Unruh radiation model. See [70].

On the other hand, in nucleus–nucleus (AA, "large systems") collisions at $\sqrt{s} \geq 15$ GeV, the so-called strangeness enhancement with respect to e^+e^- and hadronic scattering (the "small" systems) has been observed, which in the standard SHM is described by the condition $\gamma_s = 1$ in AA with respect to $\gamma_s \simeq 0.5 - 0.6$ in small systems. Moreover, the same enhancement has been detected in proton–proton collisions at large energies and in large multiplicity events [72].

The translation of *alla* Unruh (of the strangeness enhancement) requires that the different temperature for various hadronic strangeness content disappear. Indeed, $T(00)$, $T(0s)$, ... are derived from the breaking of a single string with the corresponding average acceleration and Unruh temperatures. On the other hand, as shown in reference [73], the universality among small and large systems is directly related to the initial parton density in the transverse plane.

If the initial setting is different but the collision energy and the large multiplicity cut produce initial states with similar entropy densities (i.e parton density in the transverse plane), the hadron production and other coarse-grain dynamical signatures are the same [73]. Therefore, for large parton density, there is a strong string overlap, as depicted in Figure 5.

Let us outline, in a simplified model, the mechanism that washes out the strangeness dependence of the Unruh temperature when, in a causally connected region, the parton density in the transverse plane is large.

Assume two species only: one scalar meson and one electrically neutral meson; that is, "pions" with mass m_π, and "kaons" with mass m_k and strangeness $s = 1$.

Let us consider a high-density system of quarks and antiquarks in a causally connected region for high-energy and high multiplicity events. Generalizing Equation (43), the average acceleration is given by

$$\bar{a} = \frac{N_l w_0 a_0 + N_s w_s a_s}{N_l w_0 + N_s w_s}, \tag{44}$$

where $N_l >> 1$, $N_s >> 1$ are, respectively, the number of light quarks and strange quarks.
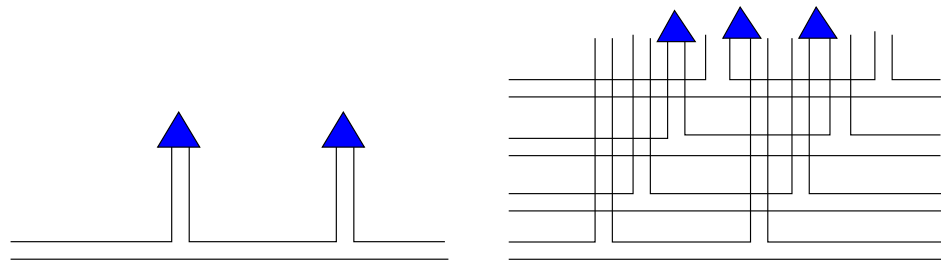
Figure 5. Left: Hadron production *alla* Unruh by a sequence of independent single string breakings. Right: Hadron production due to the overlap of different color event horizons for large parton density.

By assuming $N_l >> N_s$, after simple algebra, the average temperature, $\bar{T} = \bar{a}/2\pi$, turns out to be

$$\bar{T} = T(00) \left[1 - \frac{N_s}{N_l} \frac{w_0 + w_s}{w_0} \left(1 - \frac{T(0s)}{T(00)} \right) \right] + O[(N_s/N_l)^2], \tag{45}$$

Now, in our "world of pions and kaons", one has $N_l = 2N_\pi + N_k$ and $N_s = N_k$ and, therefore,

$$\bar{T} = T(00) \left[1 - \frac{N_k}{2N_\pi} \frac{w_0 + w_s}{w_0} \left(1 - \frac{T(0s)}{T(00)} \right) \right] + O[(N_k/N_\pi)^2]. \tag{46}$$

On the other hand, in the Hawking–Unruh-based statistical calculation, the kaon–pion ratio, N_k/N_π, depends on the equilibrium (average) temperature $\bar{T}$; that is

$$N_k/N_\pi = \frac{m_k^2}{m_\pi^2} \frac{K_2(m_k/\bar{T})}{K_2(m_\pi/\bar{T})}, \tag{47}$$

where $K_2(x)$ denotes a Hankel function of a purely imaginary argument. Therefore, one has to determine the temperature $\bar{T}$ by self-consistency of Equation (46) with Equation (47). This condition implies

$$\frac{2\left[1 - \bar{T}/T(00)\right] w_0}{\left[1 - T(0s)/T(00)\right](w_s + w_0)} = \frac{m_k^2}{m_\pi^2} \frac{K_2(m_k/\bar{T})}{K_2(m_\pi/\bar{T})}, \tag{48}$$

which can be solved numerically. For $\sigma = 0.17$ Gev^2, $m_s = 0.083$ GeV (see Figure 4), the solution gives $\bar{T}/T(00) \simeq 0.97$.

In other words, this toy model shows that the non-equilibrium condition, with species-dependent temperatures, converges to an equilibrated system, with the average temperature, $\bar{T} \simeq T(00)$, for large parton density in a causally connected region.

4. Thermal Component in the Transverse Momentum Spectra

4.1. High-Energy Hadronic Processes

The transverse momentum, p_T, and spectra of hadrons produced in high-energy collisions, can be decomposed into two components: the exponential (or "soft") component and the power (or "hard") component. Their relative strengths, in deep inelastic scattering (DIS), depend drastically on the global structure of the event. Namely, the exponential component is absent in the diffractive events characterized by a rapidity gap [74,75].

The hard component is well understood, resulting from the high-momentum transfer scattering of quarks and gluons and their subsequent fragmentations. The "soft" component is ubiquitous in high-energy collisions and appears as a thermal spectrum. In nuclear collisions, given the high number of participants involved, one may expect thermalization to take place; however, it is hard to believe that this might occur in processes such as DIS or e^+e^- annihilation.

In [76], it was found that the following parametrization well describes the hadron transverse momentum distribution, both in hadronic collisions and in deep-inelastic scattering

$$\frac{d\sigma}{p_T dp_T} = A_{therm}\, e^{-m_T/T_{th}} + A_{hard} \left(1 + \frac{m_T^2}{n\, T_{th}^2}\right)^{-n}. \tag{49}$$

This clearly defines the soft/thermal components and the hard component parameterized by T_{th}. Here, $m_T = \sqrt{m^2 + p_T^2}$.

4.2. Analog Gravity Interpretation of the Origin of the Thermal Component in the Transverse Momentum Spectra

The strength of the chromoelectric field, in a single string-breaking, is determined by the string tension, and it describes the yields of the different hadronic species. However, to discuss the transverse momentum spectra of the produced hadrons (see Section 4), one has to take into account the increasing number of gluons in the wave functions of the colliding hadrons. This can be done by the parton saturation [77], or color glass condensate [78,79] picture. In this approach, the density of partons in the transverse plane is parameterized by the saturation momentum $Q_s(s, \eta)$, which depends on the c.m.s. collision energy-squared s and (pseudo-)rapidity η.

The temperature of the radiation from the resulting Rindler event horizon is given by [5]

$$T_U = T_{th} = c\,\frac{Q_s}{2\pi}, \tag{50}$$

where c is a constant [80]. T_{th} is related to the deceleration of partons in the transverse plane; moreover, $Q_s = T$ in the parametrization of the hard component in Equation (22) [74]. Therefore, one predicts a proportionality between the T_{th} and T, which has been verified [74,75].

The established proportionality of the parameters describing the thermal and hard components of the transverse momentum spectra supports the theoretical picture in which the soft hadron production is a consequence of the quantum evaporation from the event horizon formed by the deceleration in longitudinal color fields. The absence of the thermal component in diffractive interactions lends further support to this interpretation.

5. Self-Organization and Self-Similarity

5.1. Hadronic Spectrum

The typical illustration of self-organized criticality (SOC), proposed in the pioneering work [81], is the 'avalanche dynamics' of sandpiles. There, the number $N(s)$ of avalanches of size s observed over a long period was found to vary as a power of s, $N(s) = \alpha s^{-p}$. This means that the phenomenon is scale-free, so the same structure is found, again and again, at all scales. This phenomenon is often referred to as self-similarity: the system resembles itself at all scales.

Another example of self-similarity is found when partitioning naturals. Given a natural number, $N \in \mathbb{N}$, we can *decompose* it (in mathematical jargon) into the natural, whose sum gives $N = \sum_i N_i$, with no distinction of the order of N_is entering the sum, e.g., 3 = 2 + 1 and 3 = 1 + 2 would count the same as a decomposition of 3. On the other hand, we also have *compositions* of N, which are decompositions of N in which the *order* of the terms matters. In the following, according to the 'abuse' of language in the physics literature, we shall call the decompositions "unordered partitions of the integer" (UPIs) and the compositions "ordered partitions of the integer" (OPIs).

The number of OPIs of N, say $O(N)$, can be easily computed as

$$O(N) = 2^{N-1}. \tag{51}$$

In other words, the self-similarity pattern can be phrased as "large integers consist of smaller integers, which in turn consist of still smaller integers, and so on...".

Starting with the integer N, we need to know the number $n(N,k)$ that specifies how often a given integer k occurs in the set of all OPIs of N, e.g., considering $N = 3$, we have $n(3,3) = 1$, $n(3,2) = 2$, and $n(3,1) = 5$. To apply the formalism of SOC, we associate a weight $s(k)$ to each integer. The natural choice is $s(k) = O(k) = 2^{k-1}$ and the number $n(N,k)$ we are looking for, in a scale-free scenario, is given by

$$n(N,k) = \alpha(N)[s(k)]^{-p}. \tag{52}$$

For small values of N, $n(N,k)$ is readily obtained explicitly and one finds that the critical exponent is $p \simeq 1.26$.

The previous example is immediately reminiscent of the statistical bootstrap model of Hagedorn [62,82–84]. There, we have "fireballs composed of fireballs, which in turn are composed of smaller fireballs, and so on". Indeed, its general pattern is shown to be due to an underlying structure related to the OPIs [85].

More precisely, Hagedorn's bootstrap approach proposes that a hadronic colorless state, with overall mass m, can be partitioned into structurally similar colorless states. Then, those component colorless states can be partitioned into structurally similar colorless states, and so on. If the states were at rest, the situation would be identical to the OPI just discussed. Since the constituent fireballs, though, have intrinsic motions, the number of states, $\rho(m)$, corresponding to a given mass m, is determined by the bootstrap equation, which can be asymptotically solved [83]. This gives $\rho(m) \sim m^{-a} \exp(m/T_H)$, and T_H is the solution of

$$\left(\frac{2}{3\pi}\right)\left(\frac{T_H}{m_0}\right)K_2(m_0/T_H) = 2\ln 2 - 1, \tag{53}$$

with m_0 denoting the lowest possible mass and $K_2(x)$ denoting a Hankel function of pure imaginary argument. For $m_0 = m_\pi \simeq 130$ Mev, this leads to the Hagedorn temperature

$$T_H \simeq 150 \text{MeV}, \tag{54}$$

that is, approximately, the critical hadronization temperature found in statistical QCD. The cited solution gives $a = 3$, but other exponents could also be considered.

The previous expression of $\rho(m)$ is an asymptotic solution of the bootstrap equation, which diverges for $m \to 0$; hence, it cannot hold for small masses. Using for $\rho(m)$ a result similar to the one obtained in the dual resonance model, Hagedorn proposed

$$\rho(m) = \text{const.}(1 + (m/\mu_0))^{-a} \exp(m/T_H), \tag{55}$$

where $\mu_0 \simeq 1 - 2$ GeV is a normalization constant.

We should emphasize that the form of $\rho(m)$ is entirely due to the self-organized nature of the system. That is in no way a result of thermal behavior. We expressed the slope coefficient of m in terms of the Hagedorn "temperature" only because we have the analog gravity scenarios in mind, which will soon be discussed; however, by itself, this coefficient is exclusively of combinatorial origin.

5.2. Analog Gravity Interpretation of the Partitions of Integers for BH Self-Similarity

The celebrated *self-similarity* at work in the hadronic spectrum, recalled in Section 5, is typical of many physical setups that enjoy scale invariance, such as fractals, phase transitions at the critical point, etc. [86]. Among those, BH self-similarity [87–89] is surely one of the most interesting, if one wants to probe fundamental ideas of QG.

Some aspects of BH self-similarity are understood if one recalls that the Hawking temperature, T_H, of a Planck-sized BH ($T_H \approx l_P^{-1}$, where l_P is the Planck length) could be viewed as the Hagedorn temperature in string theory [90–92]. At that temperature, BH evaporation stops and a phase transition is expected to occur, in analogy to what hap-

pens at the phase transition between the hadrons and the quark–gluon–plasma phase [93]. Nonetheless, to properly speak of self-similarity, one would need to make sense of statements, such as, "large BHs could be viewed as formed by smaller BHs, formed in turn of even smaller BHs, and so on..."

In the work [94], some steps were moved in that direction, and a link was established, in simple terms, between the spaces of BH configurations and the OPI. This, in turn, shed new light on BH self-similarity, in the plain terms of the statement quoted above. In what follows, let us comment on this.

First, the model we refer to is the so-called "quantum BH" of Mukhanov and Bekenstein [95–97]. In that approach, the area of the BH event horizon is quantized

$$A = \alpha N l_P^2,\tag{56}$$

where $N \in \mathbb{N}$ and the "it from bit" [98] choice for the proportionality factor, $\alpha = 4\ln 2$, allows for a two-level spin-1/2 system description, $\uparrow$ or $\downarrow$, per given Planck cell. With these, BH entropy, S_{BH}, can be written as

$$S_{BH} = \frac{A}{4\,l_P^2} = N\ln 2,\tag{57}$$

which is the entropy of a quantum system living in a Hilbert (configuration) space of dimension $\dim H = 2^N$, where each 2^N configuration has the same statistical weight, e.g., see [99] for this and other approaches.

Thus, on the one hand, the number of OPIs of N, $O(N) = 2^{N-1}$, whereas the number of configurations of the quantum BH is given by $C(N) = 2^N$. Therefore, if we want to relate the two ways of counting configurations, one needs to find a 2-to-1 map from the latter to the former.

In [94], this is achieved by distinguishing between BH configurations, differing not only by how many spins are up and how many are down, as in other approaches [99], but also by the *position* of the spin. The "spin-flip map", there introduced, does the job of halving the number of BH configurations in a consistent way (to associate spin states, on the one hand, and with the OPI of N, on the other hand).

The 2-to-1 map works as follows: For any one given OPI of N, it associates the two BH states that are obtained (one from the other) when all the spins that identify the given configuration are flipped, $\uparrow\leftrightarrow\downarrow$. Then, the rule that relates a given *pair* of BH (spin) configurations to a given OPI is the following (for details see [94]):

When a spin is next to an opposite spin, i.e., when $\uparrow$ is next to $\downarrow$ or when $\downarrow$ is next to $\uparrow$, in the OPI this corresponds to $1 + 1$, e.g., $(\uparrow,\downarrow,\uparrow,\ldots)$, and the spin-flips $(\downarrow,\uparrow,\downarrow,\ldots)$ both correspond in the OPI to the partition $1 + 1 + \ldots$. When the spin is likewise, it contributes with an integer that is the sum of how many times the spin does not flip, e.g., $(\uparrow,\uparrow,\downarrow,\ldots)$ and $(\downarrow,\downarrow,\uparrow,\ldots)$ correspond in the OPI to the partition $2 + \ldots$.

With these, one takes into account all possibilities; hence, the wanted 2-to-1 map from the BH configurations to the OPI (the "spin-flip map") is obtained. Having established that, we want to see how the self-similarity patterns of the OPI can be imported into the self-similarity of BHs.

To avoid overcounting some configurations or missing others, in [94], the authors constructed an operation, $\hat{+}$, which allowed obtaining the configuration space of the given BH only once, for any given partition. If we indicate with **N** such 2^N-dimensional configuration space, and $N_1 + N_2 + \cdots = N$ is a given OPI of N, such an operation must give $\mathbf{N_1}\hat{+}\mathbf{N_2}\hat{+}\cdots = \mathbf{N}$. Doing so, we establish a one-to-one correspondence between the OPI of N, and the way to combine the subspaces of **N**, corresponding to the OPI. We report here the actual definition of such an operation:

Take each partition of N, say $N_1 + N_2 = N$, and write the spin configuration space associated with the first number of the sum, $\mathbf{N_1}$. Then, take the tensor product of each representative with all of the spin configurations of $\mathbf{N_2}$, explicitly including all spin-flipped configurations. The result of

such an operation, $\mathbf{N_1}\hat{+}\mathbf{N_2}$, is all of the spin configurations of $\mathbf{N}$, with no redundant or missed configuration. The operation gives the same result for each OPI of N, including those with more than two terms. For the latter, one must start from the first term on the left, act with the second (as described), and the result needs to be acted upon with the next term, and so on, until the end.

The trivial example is $\mathbf{N} = \mathbf{N}$, where no composition is performed. The first non-trivial operation is $\mathbf{1}\hat{+}\mathbf{1}$, which originates from the partition $1 + 1 = 2$, so it must give $\mathbf{2}$:

$$\mathbf{1}\hat{+}\mathbf{1} = \uparrow \otimes \begin{matrix} \uparrow \\ \downarrow \end{matrix} = \begin{matrix} \uparrow\,\uparrow \\ \uparrow\,\downarrow \end{matrix} = \mathbf{2}\,. \tag{58}$$

Indeed, in the second-last term, the first line is one spin representative of 2, $(\uparrow,\uparrow)$, while the second line is one spin representative of $1 + 1$, $(\uparrow,\downarrow)$. The four-dimensional ($2^N = 2^2$), full configuration space, $\mathbf{2}$, is obtained when we spin-flip each final configuration: $(\uparrow,\uparrow),(\downarrow,\downarrow)$ and $(\uparrow,\downarrow),(\downarrow,\uparrow)$. Notice that this is a general feature of this operation: one can consider even just one single representative per each spin-flipped pair of the first term, perform the operation as described earlier, and then to obtain all configurations at the end of the procedure—apply the spin-flip.

We are now where we want to be. When $\mathbf{N}$ is the configuration space of a Mukhanov–Bekenstein quantum BH, we have found the BH self-similarity; in plain terms, we were searching for:

The configuration space, $\mathbf{N}$, of a BH is made of the configuration spaces of smaller BHs, which are made of configuration spaces of even smaller BHs, and again and again, until we reach N copies of $\mathbf{1}$, the configuration space of the tiniest (elementary) BH.

To any of the 2^{N-1} OPIs of N, we can associate one of the 2^{N-1} OPIs of $\mathbf{N}$

$$\sum_i N_i = N \rightarrow \hat{\sum}_i \mathbf{N_i} = \mathbf{N}\,, \quad \sum_j M_j = N \rightarrow \hat{\sum}_j \mathbf{M_j} = \mathbf{N}\,, \dots\,, \tag{59}$$

where $\hat{\sum}_i \mathbf{N_i} = \mathbf{N_1}\hat{+}\mathbf{N_2}\hat{+}\cdots$, whatever pattern we find in the OPI of N, it is found in the configuration space $\mathbf{N}$ of the BH, and then repeated for the smaller numbers, until we reach the "quantum" of the BH space, $\mathbf{1}$.

A suggestive pattern is given by

$$\mathbf{N} = \mathbf{1}\hat{+}(\mathbf{N}-\mathbf{1}) = \mathbf{1}\hat{+}(\mathbf{1}\hat{+}(\mathbf{N}-\mathbf{2})) = \mathbf{1}\hat{+}(\mathbf{1}\hat{+}(\mathbf{1}\hat{+}(\mathbf{N}-\mathbf{3}))) = \cdots = \hat{\sum}_{i=1}^{N}\mathbf{1}\,. \tag{60}$$

Here, one can say that when the configuration space of the tiniest BH, $\mathbf{1}$, is isolated from the rest, this can be repeated until the complete splitting.

As wanted, in this picture, self-similarity does not require any change of description of the degrees of freedom (e.g., from the evaporating BH to the long string [92], see also [90]). What one does there is finds patterns within the configuration space of a given fixed BH. We are not considering either BH *evaporation* or BH *merging* [100].

Let us conclude this part by saying that the constructions of [94] may solve the problem we started with. On the other hand, they lack any dynamical consideration whatsoever, as only kinematics was the concern there. No configuration is preferred to any other, by virtue of the dynamical properties of the system. In other words, all configurations were treated equally and this can only give back the entropy of (57), which, with a strong abuse of the language, since we are in a quantum BH model, is sometimes referred to as "classical entropy".

This is likely something that will be fully amended only by the long-sought-for final QG theory, see, e.g., [101], which will tell us how these fundamental (fermionic) degrees of freedom (see, e.g., [102–104]) interact, and some, $O(\ln N)$, "quantum corrections" have been put forward based on perturbative quantum considerations [105–110].

On the other hand, the simple (simplistic) approach of [94] has two advantages. First, it is based on a non-interacting (free) spin model that some authors also consider to be a viable candidate [102–104]. Second, in order to use an information–theoretical

approach, the selection of specific configurations over others is not appropriate. In fact, if a (quantum) BH has to be used as the ultimate (quantum) computer [111], then one expects all configurations to be treated equally. The actual evolution of the quantum states should not be fixed by a given spin model, but rather be governed by a specific Hamiltonian that "implements" the given "computation".

6. Conclusions

The interpretation of quark confinement as the effect of an (event) *horizon* for color degrees of freedom naturally leads to the view of hadronization as 'quantum tunneling' through such a horizon. With this view, hadron formation is the result of an Unruh phenomenon, related to the string-breaking/string formation mechanism. This is because the large-distance QCD potential generates a constant and large *acceleration*, $a \simeq 3.2 \times 10^{33}$ m/s^2, which is precisely what we need for a measurable Unruh effect, $T_U \sim 4 \times 10^{11}$K ~ 170 MeV.

This opens up the way for a clear explanation of the thermal behaviors of both arenas—hadron physics and BH physics. For instance, this immediately explains why the hadronization temperature, T_h, is universal when seen as a T_U. Indeed, T_h is found to be the same for small and large initial collision settings, whereas T_U is fixed, once and for all, by the value of the acceleration, a. This also explains why hadrons are born in equilibrium.

In fact, the Hawking–Unruh radiation is an example of a *stochastic* rather than *kinetic* equilibrium. The reason behind the randomization is not repeated (as well as casual collisions among particles), but rather the quantum entanglement between the degrees of freedom on the two sides of the barrier to the information transfer, which is the event horizon. The temperature is then determined by the strength of the "confining" field.

In the chromodynamics counterpart of this phenomenon, described in this review, the ensemble of all produced hadrons, averaged over all events, leads to the same equilibrium distribution as obtained in the hadronic matter by kinetic equilibration. For a very high-energy collision, with a high average multiplicity, even one event alone can provide such equilibrium. The destruction of memory, which in kinetic equilibration is achieved through many successive collisions, is here automatically provided by the tunneling process.

The above are the physical fundamental aspects common to both types of phenomena. On this, the analogy can be solidly established, and many results can be obtained, i.e., the string-breaking and BH entropy analogies, which reproduce the "magic numbers" characterizing the freeze-out curve; the strangeness production, at low parton density, which is due to different Unruh temperatures in the single string-breaking; at high-energy and multiplicity, the large parton density, in the transverse plane, which removes the different temperatures by string (or color event horizon) overlap, giving the strangeness enhancement; or self-similar behavior, characteristic of the hadronic production, which has driven research into the self-similarity of BH configurations.

Let us then close on an optimistic note, by stating that this new and original analog system of QG has many other results to grasp.

In particular, Unruh radiation should exhibit both spatial and temporal coherence, reflecting its quantum origin. In our case, the spatial coherence should be observable by probing the phase correlation between particle jets. This correlation exists in the gravitational case, although it cannot be detected since one particle of the pair remains trapped inside the event horizon. Indeed, in the condensed matter analog of the Unruh effect, this correlation has been observed [112].

Another interesting aspect concerns the relation between 'de-confinement' and restoration of the chiral symmetry. The Rindler metric corresponds to the near-horizon approximation of a black-hole metric. On the other hand, in the near-horizon approximation, the field theory becomes conformal and effectively two-dimensional. Therefore, there is no way, in the near-horizon approximation, to maintain a physical scale generated by symmetry

breaking. From this point of view, the Unruh hadronization temperature and the critical temperature of the restoration of chiral symmetry are deeply related.

Note

[1] In fact, different physical systems, governed by different Hamiltonians, Lagrangians, and equations of motion (dynamics) may exhibit analog features, such as the emergence of some sort of horizon, as with the vast majority of cases used to probe the Hawking–Unruh phenomenon [1]. This is similar to taking a snapshot of the evolution of the analog system, precisely when this "looks like" the target system (or, we believe it should "look like" the target system). With this, we can study the behavior of the target system using the analog system at that particular stage of the evolution. It is much more important though to be able to keep going, even just a little bit. Namely, it is important that the evolution of the analog system is similar to the one of the target system, at least in certain conditions and within a limited range. When this happens, we have a much better analog that can furnish much more information on the target system (these are the analogs introduced in the famous Feynman lecture of electrostatics [4]). This is particularly important when one wants to face issues, such as black-hole (BH) evaporation, which is a phenomenon intimately associated with the dynamics of the gravitational field and something impossible to capture in a single "snapshot".

References

1. Barceló, C.; Liberati, S.; Visser, M. Analogue Gravity. *Living Rev. Relativ.* **2005**, *8*, 12. [CrossRef] [PubMed]
2. Muñoz de Nova, J.R.; Golubkov, K.; Kolobov, V.I.; Steinhauer, J. Observation of thermal Hawking radiation and its temperature in an analogue black hole. *Nature* **2019**, *569*, 688–691. [CrossRef] [PubMed]
3. Acquaviva, G.; Iorio, A.; Pais, P.; Smaldone, L. Hunting Quantum Gravity with Analogs: The case of graphene. *Universe* **2022**, *8*, 455. [CrossRef]
4. Feynman, R.; Leighton, R.; Sands, M. *The Feynman Lectures on Physics*; Number v. 2 in Addison-Wesley World Student Series; Addison-Wesley: Reading, MA, USA, 1963.
5. Kharzeev, D.; Tuchin, K. From color glass condensate to quark–gluon plasma through the event horizon. *Nucl. Phys. A* **2005**, *753*, 316–334. [CrossRef]
6. Castorina, P.; Kharzeev, D.; Satz, H. Thermal hadronization and Hawking–Unruh radiation in QCD. *Eur. Phys. J. C* **2007**, *52*, 187. [CrossRef]
7. Wald, R.M. Black hole entropy is the Noether charge. *Phys. Rev. D* **1993**, *48*, R3427–R3431. [CrossRef] [PubMed]
8. Chen, P.; Tajima, T. Testing Unruh Radiation with Ultraintense Lasers. *Phys. Rev. Lett.* **1999**, *83*, 256–259. [CrossRef]
9. Schützhold, R.; Schaller, G.; Habs, D. Signatures of the Unruh Effect from Electrons Accelerated by Ultrastrong Laser Fields. *Phys. Rev. Lett.* **2006**, *97*, 121302. [CrossRef]
10. Schützhold, R.; Schaller, G.; Habs, D. Tabletop Creation of Entangled Multi-keV Photon Pairs and the Unruh Effect. *Phys. Rev. Lett.* **2008**, *100*, 091301. [CrossRef]
11. Kim, C.M.; Kim, S.P. Unruh effect and Schwinger pair creation under extreme acceleration by ultraintense lasers. *arXiv* **2017**. [CrossRef]
12. O'Raifeartaigh, L.; Sreedhar, V. The Maximal Kinematical Invariance Group of Fluid Dynamics and Explosion–Implosion Duality. *Ann. Phys.* **2012**, *293*, 215–227. [CrossRef]
13. Sreedhar, V.V.; Virmani, A. Maximal Kinematical Invariance Group of Fluid Dynamics and Applications. *Universe* **2022**, *8*, 319. [CrossRef]
14. Drori, J.; Rosenberg, Y.; Bermudez, D.; Silberberg, Y.; Leonhardt, U. Observation of Stimulated Hawking Radiation in an Optical Analogue. *Phys. Rev. Lett.* **2019**, *122*, 010404. [CrossRef]
15. Iorio, A. Weyl-gauge symmetry of graphene. *Ann. Phys.* **2011**, *326*, 1334–1353. [CrossRef]
16. Iorio, A. Using Weyl symmetry to make graphene a real lab for fundamental physics. *Eur. Phys. J. Plus* **2102**, *127*, 156. [CrossRef]
17. Iorio, A.; Lambiase, G. The Hawking–Unruh phenomenon on graphene. *Phys. Lett. B* **2012**, *716*, 334–337. [CrossRef]
18. Iorio, A.; Lambiase, G. Quantum field theory in curved graphene spacetimes, Lobachevsky geometry, Weyl symmetry, Hawking effect, and all that. *Phys. Rev. D* **2014**, *90*, 025006. [CrossRef]
19. Iorio, A. Curved spacetimes and curved graphene: A status report of the Weyl symmetry approach. *Int. J. Mod. Phys. D* **2015**, *24*, 1530013, [CrossRef]
20. Iorio, A.; Pais, P. Revisiting the gauge fields of strained graphene. *Phys. Rev. D* **2015**, *92*, 125005. [CrossRef]

21. Iorio, A.; Pais, P. (Anti-)de Sitter, Poincaré, Super symmetries, and the two Dirac points of graphene. *Ann. Phys.* **2018**, *398*, 265–286. [CrossRef]
22. Iorio, A.; Pais, P. Generalized uncertainty principle in graphene. *J. Phys. Conf. Ser.* **2019**, *1275*, 012061. [CrossRef]
23. Iorio, A.; Pais, P.; Elmashad, I.A.; Ali, A.F.; Faizal, M.; Abou-Salem, L.I. Generalized Dirac structure beyond the linear regime in graphene. *Int. J. Mod. Phys. D* **2018**, *27*, 1850080. [CrossRef]
24. Ciappina, M.F.; Iorio, A.; Pais, P.; Zampeli, A. Torsion in quantum field theory through time-loops on Dirac materials. *Phys. Rev. D* **2020**, *101*, 036021. [CrossRef]
25. Iorio, A.; Lambiase, G.; Pais, P.; Scardigli, F. Generalized uncertainty principle in three-dimensional gravity and the BTZ black hole. *Phys. Rev. D* **2020**, *101*, 105002. [CrossRef]
26. Hawking, S.W. Particle creation by black holes. *Commun. Math. Phys.* **1975**, *43*, 199–220. [CrossRef]
27. Unruh, W.G. Notes on black-hole evaporation. *Phys. Rev. D* **1976**, *14*, 870–892. [CrossRef]
28. Crispino, L.C.B.; Higuchi, A.; Matsas, G.E.A. The Unruh effect and its applications. *Rev. Mod. Phys.* **2008**, *80*, 787–838. [CrossRef]
29. Guedes, T.L.M.; Kizmann, M.; Seletskiy, D.V.; Leitenstorfer, A.; Burkard, G.; Moskalenko, A.S. Spectra of Ultrabroadband Squeezed Pulses and the Finite-Time Unruh-Davies Effect. *Phys. Rev. Lett.* **2019**, *122*, 053604. [CrossRef]
30. Smolyaninov, I.I. Giant Unruh effect in hyperbolic metamaterial waveguides. *Opt. Lett.* **2019**, *44*, 2224–2227. [CrossRef] [PubMed]
31. Kalinski, M. Hawking radiation from Trojan states in muonic Hydrogen in strong laser field. *Laser Phys.* **2005**, *15*, 1357–1361.
32. Recami, E.; Castorina, P. On quark confinement: Hadrons as «strong black holes». *Lett. Al Nuovo Cimento (1971–1985)* **1976**, *15*, 347–350. [CrossRef]
33. Salam, A.; Strathdee, J. Confinement through tensor gauge fields. *Phys. Rev. D* **1978**, *18*, 4596–4609. [CrossRef]
34. Di Giacomo, A. Understanding Color Confinement. *EPJ Web Conf.* **2014**, *70*, 00019. [CrossRef]
35. Castorina, P.; Grumiller, D.; Iorio, A. Exact string black hole behind the hadronic Rindler horizon? *Phys. Rev. D* **2008**, *77*, 124034. [CrossRef]
36. Parikh, M.K.; Wilczek, F. Hawking Radiation As Tunneling. *Phys. Rev. Lett.* **2000**, *85*, 5042–5045. [CrossRef] [PubMed]
37. Vanzo, L.; Acquaviva, G.; Criscienzo, R.D. Tunnelling methods and Hawking's radiation: Achievements and prospects. *Class. Quantum Gravity* **2011**, *28*, 183001. [CrossRef]
38. Srednicki, M. Entropy and area. *Phys. Rev. Lett.* **1993**, *71*, 666–669. [CrossRef]
39. Terashima, H. Entanglement entropy of the black hole horizon. *Phys. Rev. D* **2000**, *61*, 104016. [CrossRef]
40. Iorio, A.; Lambiase, G.; Vitiello, G. Entangled quantum fields near the event horizon and entropy. *Ann. Phys.* **2004**, *309*, 151–165. [CrossRef]
41. Bekenstein, J.D. Black Holes and Entropy. *Phys. Rev. D* **1973**, *7*, 2333–2346. [CrossRef]
42. Hawking, S.W. Black hole explosions? *Nature* **1974**, *248*, 30–31. [CrossRef]
43. Laflamme, R. Entropy of a Rindler wedge. *Phys. Lett. B* **1987**, *196*, 449–450. [CrossRef]
44. Page, D.N. Information in black hole radiation. *Phys. Rev. Lett.* **1993**, *71*, 3743–3746. [CrossRef]
45. Castorina, P.; Iorio, A.; Lanteri, D.; Lukeš, P. Gluon shadowing and nuclear entanglement entropy. *Int. J. Mod. Phys. E* **2021**, *30*, 2150010. [CrossRef]
46. Kharzeev, D.E.; Levin, E.M. Deep inelastic scattering as a probe of entanglement. *Phys. Rev. D* **2017**, *95*, 114008. [CrossRef]
47. Parentani, R.; Massar, S. Schwinger mechanism, Unruh effect, and production of accelerated black holes. *Phys. Rev. D* **1997**, *55*, 3603–3613. [CrossRef]
48. Gabriel, C.; Spindel, P. Quantum Charged Fields in (1+1) Rindler Space. *Ann. Phys.* **2000**, *284*, 263–335. [CrossRef]
49. Narozhny, N.; Mur, V.; Fedotov, A. Pair creation by homogeneous electric field from the point of view of an accelerated observer. *Phys. Lett. A* **2003**, *315*, 169–174. [CrossRef]
50. De Gill, A.; Singleton, D.; Akhmedova, V.; Pilling, T. A WKB-like approach to Unruh radiation. *Am. J. Phys.* **2010**, *78*, 685–691. [CrossRef]
51. Becattini, F. A thermodynamical approach to hadron production ine+ e- collisions. *Z. Für Phys. C Part. Fields* **1995**, *69*, 485–492. [CrossRef]
52. Cleymans, J.; Satz, H.; Suhonen, E.; Von Oertzen, D. Strangeness production in heavy ion collisions at finite baryon number density. *Phys. Lett. B* **1990**, *242*, 111–114. [CrossRef]
53. Andronic, A.; Braun-Munzinger, P.; Redlich, K.; Stachel, J. Decoding the phase structure of QCD via particle production at high energy. *Nature* **2018**, *561*, 321–330. [CrossRef]
54. Letessier, J.; Rafelski, J.; Tounsi, A. Gluon production, cooling, and entropy in nuclear collisions. *Phys. Rev. C* **1994**, *50*, 406–409. [CrossRef] [PubMed]
55. Magas, V.; Satz, H. Conditions for confinement and freeze-out. *Eur. Phys. J. C-Part. Fields* **2003**, *32*, 115–119. [CrossRef]
56. Cleymans, J.; Redlich, K. Unified Description of Freeze-Out Parameters in Relativistic Heavy Ion Collisions. *Phys. Rev. Lett.* **1998**, *81*, 5284–5286. [CrossRef]
57. Braun-Munzinger, P.; Stachel, J. Particle ratios, equilibration and the QCD phase boundary. *J. Phys. G Nucl. Part. Phys.* **2002**, *28*, 1971–1976. [CrossRef]
58. Cleymans, J.; Oeschler, H.; Redlich, K.; Wheaton, S. Transition from baryonic to mesonic freeze-out. *Phys. Lett. B* **2005**, *615*, 50–54. [CrossRef]

59. Tawfik, A. Influence of strange quarks on the QCD phase diagram and chemical freeze-out. *J. Phys. G Nucl. Part. Phys.* **2005**, *31*, S1105–S1110. [CrossRef]

60. Lüscher, M.; Münster, G.; Weisz, P. How thick are chromo-electric flux tubes? *Nucl. Phys. B* **1981**, *180*, 1–12. [CrossRef]

61. Yndurain, F. *The Theory of Quark and Gluon Interactions*; Theoretical and Mathematical Physics, Springer: Berlin/Heidelberg, Germany, 2013.

62. Hagedorn, R. Statistical thermodynamics of strong interactions at high energies. *Nuovo Cimento Suppl.* **1965**, *3*, 147–186.

63. Hagedorn, R. Thermodynamics of strong interactions. *Cargese Lect. Phys.* **1973**, *6*, 643–716.

64. Castorina, P.; Iorio, A.; Satz, H. Hadron freeze-out and Unruh radiation. *Int. J. Mod. Phys. E* **2015**, *24*, 1550056. [CrossRef]

65. Solodukhin, S.N. Entanglement Entropy of Black Holes. *Living Rev. Relativ.* **2011**, *14*, 8. [CrossRef] [PubMed]

66. Castorina, P.; Iorio, A. Confinement horizon and QCD entropy. *Int. J. Mod. Phys. A* **2018**, *33*, 1850211. [CrossRef]

67. Becattini, F.; Manninen, J.; Gaździcki, M. Energy and system size dependence of chemical freeze-out in relativistic nuclear collisions. *Phys. Rev. C* **2006**, *73*, 044905. [CrossRef]

68. Grumiller, D.; Kummer, W.; Vassilevich, D. Dilaton gravity in two dimensions. *Phys. Rep.* **2002**, *369*, 327–430. [CrossRef]

69. Birmingham, D.; Gupta, K.S.; Sen, S. Near-horizon conformal structure of black holes. *Phys. Lett. B* **2001**, *505*, 191–196. [CrossRef]

70. Becattini, F.; Castorina, P.; Manninen, J.; Satz, H. The thermal production of strange and nonstrange hadrons in e+ e- collisions. *Eur. Phys. J. C* **2008**, *56*, 493–510. [CrossRef]

71. Becattini, F.; Castorina, P.; Milov, A.; Satz, H. A comparative analysis of statistical hadron production. *Eur. Phys. J. C* **2010**, *66*, 377–386. [CrossRef]

72. Adam, J.; Adamová, D.; Aggarwal, M.M.; Rinella, G.A.; Agnello, M.; Agrawal, N.; Ahammed, Z.; Ahmad, S.; Ahn, S.U.; Aiola, S.; et al. Enhanced production of multi-strange hadrons in high-multiplicity proton–proton collisions. *Nat. Phys.* **2017**, *13*, 535–539. [CrossRef]

73. Castorina, P.; Iorio, A.; Lanteri, D.; Satz, H.; Spousta, M. Universality in hadronic and nuclear collisions at high energy. *Phys. Rev. C* **2020**, *101*, 054902. [CrossRef]

74. Bylinkin, A.A.; Kharzeev, D.E.; Rostovtsev, A.A. The origin of thermal component in the transverse momentum spectra in high energy hadronic processes. *Int. J. Mod. Phys. E* **2014**, *23*, 1450083. [CrossRef]

75. Baker, O.K.; Kharzeev, D.E. Thermal radiation and entanglement in proton-proton collisions at energies available at the CERN Large Hadron Collider. *Phys. Rev. D* **2018**, *98*, 054007. [CrossRef]

76. Bylinkin, A.A.; Rostovtsev, A.A. Parametrization of the shape of hadron-production spectra in high-energy particle interactions. *Phys. At. Nucl.* **2012**, *75*, 999–1005. [CrossRef]

77. Gribov, L.; Levin, E.; Ryskin, M. Semihard processes in QCD. *Phys. Rep.* **1983**, *100*, 1–150. [CrossRef]

78. McLerran, L.; Venugopalan, R. Computing quark and gluon distribution functions for very large nuclei. *Phys. Rev. D* **1994**, *49*, 2233–2241. [CrossRef]

79. McLerran, L.; Venugopalan, R. Gluon distribution functions for very large nuclei at small transverse momentum. *Phys. Rev. D* **1994**, *49*, 3352–3355. [CrossRef]

80. Kharzeev, D.; Levin, E.; Tuchin, K. Multiparticle production and thermalization in high-energy QCD. *Phys. Rev. C* **2007**, *75*, 044903. [CrossRef]

81. Bak, P.; Tang, C.; Wiesenfeld, K. Self-organized criticality: An explanation of the 1/f noise. *Phys. Rev. Lett.* **1987**, *59*, 381–384. [CrossRef]

82. Frautschi, S. Statistical Bootstrap Model of Hadrons. *Phys. Rev. D* **1971**, *3*, 2821–2834. [CrossRef]

83. Nahm, W. Analytical solution of the statistical bootstrap model. *Nucl. Phys. B* **1972**, *45*, 525–553. [CrossRef]

84. Hagedorn, R.; Rafelski, J. Analytic structure and explicit solution of an important implicit equation. *Commun. Math. Phys.* **1982**, *83*, 563–578. [CrossRef]

85. Blanchard, P.; Fortunato, S.; Satz, H. The Hagedorn temperature and partition thermodynamics. *Eur. Phys. J. C-Part. Fields* **2004**, *34*, 361–366. [CrossRef]

86. Zinn-Justin, J. *Quantum Field Theory and Critical Phenomena*; International series of monographs on physics; Clarendon Press: Oxford, UK, 2002.

87. Harms, B.; Leblanc, Y. Statistical mechanics of black holes. *Phys. Rev. D* **1992**, *46*, 2334–2340. [CrossRef] [PubMed]

88. Harms, B.; Leblanc, Y. Statistical mechanics of extended black objects. *Phys. Rev. D* **1993**, *47*, 2438–2445. [CrossRef] [PubMed]

89. Huang, W.H. Microcanonical statistics of black holes and the bootstrap condition. *Phys. Rev. D* **2000**, *62*, 043002. [CrossRef]

90. Veneziano, G. The Hagedorn Spectrum and the Dual Resonance Model: An Old Love Affair. In *Melting Hadrons, Boiling Quarks—From Hagedorn Temperature to Ultra-Relativistic Heavy-Ion Collisions at CERN: With a Tribute to Rolf Hagedorn*; Rafelski, J., Ed.; Springer International Publishing: Cham, Switzerland, 2016; pp. 69–74. [CrossRef]

91. Susskind, L.; Thorlacius, L.; Uglum, J. The stretched horizon and black hole complementarity. *Phys. Rev. D* **1993**, *48*, 3743–3761. [CrossRef]

92. Susskind, L.; Lindesay, J. *An Introduction to Black Holes, Information and the String Theory Revolution*; World Scientific: London, UK, 2004. [CrossRef]

93. Cabibbo, N.; Parisi, G. Exponential hadronic spectrum and quark liberation. *Phys. Lett. B* **1975**, *59*, 67–69. [CrossRef]

94. Castorina, P.; Iorio, A.; Smaldone, L. Quantum black holes, partition of integers and self-similarity. *Mod. Phys. Lett. A* **2022**. [CrossRef]

95. Mukhanov, V.F. Are black holes quantized? *Sov. J. Exp. Theor. Phys. Lett.* **1986**, *44*, 63–66.

96. Bekenstein, J.D.; Mukhanov, V. Spectroscopy of the quantum black hole. *Phys. Lett. B* **1995**, *360*, 7–12. [CrossRef]

97. Bekenstein, J.D. Quantum Black Holes as Atoms. In *Recent Developments in Theoretical and Experimental General Relativity, Gravitation, and Relativistic Field Theories*; World Scientific: London, UK, 1999; p. 92.

98. Wheeler, J. *Information, Physics, Quantum: The Search for Links*; Pamphlets on Physics, Physics Department, Princeton University: Princeton, NJ, USA, 1989.

99. Kiefer, C. Aspects of Quantum Black Holes. *J. Physics: Conf. Ser.* **2020**, *1612*, 012017. [CrossRef]

100. Abbott, B.P.; Abbott, R.; Abbott, T.D.; Abernathy, M.R.; Acernese, F.; Ackley, K.; Adams, C.; Adams, T.; Addesso, P.; Adhikari, R.X.; et al. Observation of Gravitational Waves from a Binary Black Hole Merger. *Phys. Rev. Lett.* **2016**, *116*, 061102. [CrossRef] [PubMed]

101. Rovelli, C.; Press, C.U.; Landshoff, P.; Nelson, D.; Sciama, D.; Weinberg, S. *Quantum Gravity*; Cambridge Monographs on Mathematical Physics, Cambridge University Press: Cambridge, UK, 2004.

102. Acquaviva, G.; Iorio, A.; Scholtz, M. On the implications of the Bekenstein bound for black hole evaporation. *Ann. Phys.* **2017**, *387*, 317–333. [CrossRef]

103. Iorio, A. Two arguments for more fundamental building blocks. *J. Phys. Conf. Ser.* **2019**, *1275*, 012013. [CrossRef]

104. Acquaviva, G.; Iorio, A.; Smaldone, L. Bekenstein bound from the Pauli principle. *Phys. Rev. D* **2020**, *102*, 106002. [CrossRef]

105. Kaul, R.K.; Majumdar, P. Logarithmic Correction to the Bekenstein-Hawking Entropy. *Phys. Rev. Lett.* **2000**, *84*, 5255–5257. [CrossRef]

106. Gupta, K.S.; Sen, S. Further evidence for the conformal structure of a Schwarzschild black hole in an algebraic approach. *Phys. Lett. B* **2002**, *526*, 121–126. [CrossRef]

107. Ghosh, A.; Mitra, P. Log correction to the black hole area law. *Phys. Rev. D* **2005**, *71*, 027502. [CrossRef]

108. Majhi, A.; Majumdar, P. 'Quantum hairs' and entropy of the quantum isolated horizon from Chern–Simons theory. *Class. Quantum Gravity* **2014**, *31*, 195003. [CrossRef]

109. Singleton, D.; Vagenas, E.C.; Zhu, T. Self-similarity, conservation of entropy/bits and the black hole information puzzle. *J. High Energy Phys.* **2014**, *2014*, 74. [CrossRef]

110. Ong, Y.C. GUP-corrected black hole thermodynamics and the maximum force conjecture. *Phys. Lett. B* **2018**, *785*, 217–220. [CrossRef]

111. Lloyd, S. Ultimate physical limits to computation. *Nature* **2000**, *406*, 1047–1054. [CrossRef] [PubMed]

112. Hu, J.; Feng, L.; Zhang, Z.; Chin, C. Quantum simulation of Unruh radiation. *Nat. Phys.* **2019**, *15*, 785–789. [CrossRef]